BNL-224134-2023-TECH

EIC-ADD-TN-41

HSR transition jump optics in the September 2022 layout

S. Peggs

March 2023

Electron-Ion Collider

Brookhaven National Laboratory

U.S. Department of Energy

USDOE Office of Science (SC), Nuclear Physics (NP) (SC-26)

DISCLAIMER

BNL-224134-2023-TECH
EIC-ADD-TN-41

HSR transition jump optics in the September 2022 layout

S. Peggs, A. Drees, H. Lovelace III, G. Robert-Demolaize.

March 14, 2023

Contents

Abstract

Transition is crossed during acceleration in the Hadron Storage Ring (HSR) for all species other than protons. A first-order transition jump scheme manipulates the value of the optical quantity γ_T and distorts the optics of the HSR around the time that the beam energy γ_{beam} crosses the nominal transition value γ_{T0}. The jump scheme in the Relativistic Heavy Ion Collider (RHIC) uses 48 jump quads, driven by 12 bi-polar power supplies that each drive 4 quads in series. Ten of those 48 are eliminated in the preliminary September 2022 HSR layout (EIC-HSR-220921a) that was developed from RHIC with no initial regard for transition crossing.

This note analyzes the performance of the 38-quad HSR scheme, by comparison with the 48-quad RHIC scheme. It is concerned only with optics – the manipulation and response of Twiss functions and related quantities – and not with beams. This evaluation is a necessary first step before enhancing the transition jump scheme **to restore RHIC performance in the HSR.** Eventually full beam simulations of transition crossing need to be performed.

1 Introduction

An on-momentum particle passes through transition at time $t = 0$, when

$$\gamma_{beam}(t, 0) \;=\; \gamma_{T0} + \gamma' \, t \tag{1}$$

where $\gamma' = d\gamma/dt$ is the acceleration ramp rate. More generally, a particle that is off-momentum by $\delta = \Delta p/p$ crosses transition when

$$\gamma_{beam}(t, \delta) \;=\; \gamma_{T0} \tag{2}$$

The maximum time delay or advance from the nominal crossing time – the so-called nonlinear time $\pm T_{NL}$ – occurs for a particle with $\delta = \pm\delta_{MAX}$ at the edge of the momentum distribution of the beam [1, 2]. It depends on the optics through

$$T_{NL} \;=\; (\alpha_1 \;+\; \frac{3}{2}\beta_T^2) \;\; \frac{\gamma_{T0}}{\gamma'} \;\; \delta_{MAX} \tag{3}$$

where the "nonlinear parameter" α_1 is the quadratic coefficient in the polynomial expansion of the change in total circumference ΔC with respect to δ

$$\frac{\Delta C}{C} \;=\; \frac{\delta}{\gamma_{T0}} \left(1 + \alpha_1 \delta + O(\delta^2)\right) \tag{4}$$

and C is the nominal circumference. Equation 3 shows that moving the nonlinear parameter closer to its ideal value of $\alpha_1 \approx -1.5$ encourages all ions to cross transition in unison [3, 4].

The value of α_1 varies with the optics and with the two chromaticities. RHIC optics with $\alpha_1 = -3/2$ can be achieved with values of $\beta^* \approx 3$ m in both planes at each Interaction Point (IP). However, such small values of β^* makes the beam uncomfortably large in the focusing triplets. Further, the tune variation with $\Delta\gamma_T$ becomes stronger when β^* is smaller. In a compromise, RHIC routinely crosses transition with $\beta^* = 5$ m at all IPs. Even when $\alpha_1 = -3/2$ optics are possible and convenient, it is still necessary to manipulate $\Delta\gamma_T(t)$, where

$$\gamma_T(t) \;=\; \gamma_{T0} + \Delta\gamma_T(t) \tag{5}$$

The optical quantity $\Delta\gamma_T$ must vary from a maximum positive value to a minimum negative value over a range of as much as

$$-1 \;<\; \Delta\gamma_T \;<\; +1 \tag{6}$$

in a time span of $\pm T_{NL}$ around the nominal transition crossing.

This note doesn't care about beam or time. It is concerned only with the optics of a lattice at a stationary point in time – at a "stone" or a "strength vector" in RHIC and HSR jargon. The values of γ_{beam} and γ' do not enter in what follows, except among the transition crossing parameters listed in Table 1. Nor does α_1 enter any further, even though it, like γ_T, is an optical quantity.

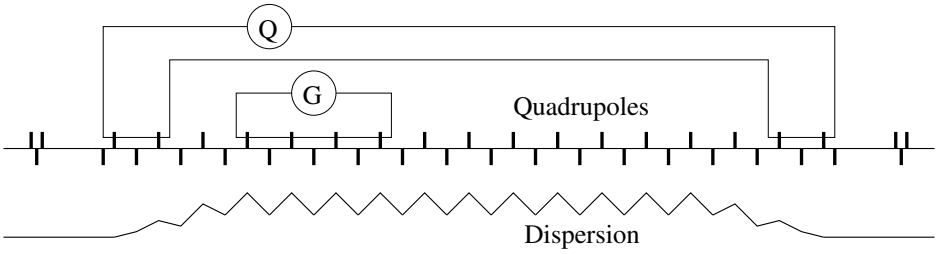

Figure 1: G and Q families of jump quads in one of the 6 RHIC arcs.

2 Power supply sensitivities $d\gamma_T/dq$ and dQ_H/dq

In RHIC $\Delta\gamma_T$ is manipulated using 48 jump quads, driven by 12 fast bi-polar power supplies that are connected in series to 4 quads, as sketched in Figure 1. In each arc the "G" set of jump quads (at high dispersion locations) mainly controls $\Delta\gamma_T$, while a second "Q" set (in low dispersion locations) mainly compensates for the shift in horizontal tune ΔQ_H. Each of the jump quads is one layer of a four layer iron-free superconducting corrector, in a Corrector-Quadrupole-Sextupole (CQS) cryomodule.

The strength of power supply number p is written as the integrated strength q_p of one of its quads

$$q_p \;=\; k_p L \;=\; \frac{1}{f_p} \tag{7}$$

where k_p is the geometric strength of the quad, L is its length, and f_p is its focal length. It can be shown [6] that to first order a set of jump quads powered at the same strength q_p delivers

$$\Delta\gamma_T \;=\; q_p \cdot \frac{\gamma_{T0}^3}{2C} \sum_{p \text{ quads}} \eta^2 \tag{8}$$

where C is the accelerator circumference and η is the dispersion at each quad. Similarly, power supply p shifts the horizontal tune Q_H according to

$$\Delta Q_H \;=\; q_p \cdot \frac{1}{4\pi} \sum_{p \text{ quads}} \beta_H \tag{9}$$

Parameter	**Units**	**RHIC**	**HSR**
Layout		Yellow, 2023	EIC-HSR-220921a
Optics		$\beta^* = 5$ m	"275", 2 collisions
Circumference C	m	3833.845	3833.888
Number of jump quads		48	38
Gamma transition γ_{T0}		23.33	22.20
Gold rigidity at transition ($B\rho$)	Tm	180.03	171.76
Maximum jump quad strength $\lvert B'L\rvert$	T	1.5	
$\lvert q\rvert$	m^{-1}	0.00833	0.00877
Phase advance per FODO cell, H	2π	0.229	0.219
V	2π	0.241	0.226
Tune, Q_H		28.238	28.228
Q_V		29.228	27.210
Chromaticity, C_H		$-2 \rightarrow +2$	
C_V		$-2 \rightarrow +2$	
Gold atomic number Z		79	
Gold atomic weight A		196.97	
Maximum momentum spread δ_{max}		0.00432	
RF voltage	kV	200	
Acceleration ramp rate γ'	s^{-1}	0.278	
Harmonic number h		360	315

Table 1: Transition crossing parameters in RHIC and HSR, with gold beam. There are only minor differences in the values of the two sets of parameters, and so the optical performance requirements for HSR are essentially identical to those in RHIC. The maximum absolute jump quad strength $|q|$ occurs when a current of 50 A delivers an integrated strength of $|B'L| = 1.5$ T, at the appropriate transition rigidity [5].

The two linear sensitivities of primary interest for each power supply

$$\begin{aligned} S_{G,p} &\equiv \frac{d\gamma_T}{dq_p} \\ S_{Q,p} &\equiv \frac{dQ_H}{dq_p} \end{aligned} \tag{10}$$

therefore have values of

$$\begin{aligned} S_{G,p} &= \frac{\gamma_{T0}^3}{2C} \sum_{p \text{ quads}} \eta^2 \\ S_{Q,p} &= \frac{1}{4\pi} \sum_{p \text{ quads}} \beta_H \end{aligned} \tag{11}$$

Both sensitivities $S_{G,p}$ and $S_{Q,p}$ have the dimension of length.

Equations 8 and 9 show that jump quads at large dispersion locations affect both $\Delta\gamma_T$ and ΔQ_H, while those at small dispersion locations with $\eta \approx 0$ mostly affect ΔQ_H, with little effect on $\Delta\gamma_T$. Hence it is natural to separate jump quads into families at high and low dispersion locations, in order to orthogonalize the control of ΔQ_H and $\Delta\gamma_T$ as far as possible. For example, in a "2-knob solution" all 6 G power supplies have strength q_G, and all 6 Q power supplies have strength q_Q.

In routine operation RHIC uses a 4-knob solution that groups 12 power supplies into 4 sets of 3 power supplies, for a total of 4 independent variables. Two knobs control the G sets of jump quads, and two control Q sets. 4-knob solutions are important when nonlinearities (in $\Delta\gamma_T$ and ΔQ_H versus strength q) come into play. Nonetheless, the 4 values used in RHIC operations usually differ only slightly from the values that are found in the 2-knob linear solution described here. A 2-knob scenario conveniently enables the comparison of the contemporary RHIC-48 performance with the HSR-38 performance in the EIC-HSR-220921a layout.

The linear contributions to $\Delta\gamma_T$ and ΔQ_H in a 2-knob solution are

$$\begin{pmatrix} \Delta\gamma_T \\ \Delta Q_H \end{pmatrix} = T \begin{pmatrix} q_G \\ q_Q \end{pmatrix} \tag{12}$$

where the 2-knob T matrix elements in

$$T = \begin{pmatrix} T_{GG} & T_{GQ} \\ T_{QG} & T_{QQ} \end{pmatrix} = \begin{pmatrix} \sum S_{G,p} & \sum S_{G,p} \\ \sum S_{Q,p} & \sum S_{Q,p} \end{pmatrix} \tag{13}$$

are found using Equation 11. The sums are over all G supplies for T matrix elements T_{GG} and T_{QG}, and over all Q supplies for T_{GQ} and T_{QQ}. The 2-knob solution is found by inverting the matrix T

$$\begin{pmatrix} q_G \\ q_Q \end{pmatrix} = T^{-1} \begin{pmatrix} \Delta\gamma_T \\ \Delta Q_H \end{pmatrix} \tag{14}$$

to deliver the 2 strengths q_G and q_Q.

Usually the desired ΔQ_H is zero, in which case

$$\Delta Q_H = 0 = T_{QG} \cdot q_G + T_{QG} \cdot q_Q \tag{15}$$

so that

$$q_Q = -\left(\frac{T_{QG}}{T_{QQ}}\right) q_G \tag{16}$$

and

$$q_G = \frac{\Delta\gamma_T}{\left(T_{GG} - T_{GQ} \cdot \left(\frac{T_{QG}}{T_{QQ}}\right)\right)} \tag{17}$$

Equation 16 shows that the ratio of q_Q to q_G is a constant in this linear model, when $\Delta Q_H = 0$.

3 Optical distortions and jump quad spacing

Jump quads at horizontal phase locations ϕ_i cause a first order total horizontal beta wave of

$$\frac{\Delta\beta_H}{\beta_H} = \frac{1}{2\ \sin(2\pi Q_H)} \sum_i q_i \beta_{Hi}\ \cos(2|\phi - \phi_i| - 2\pi Q_H) \tag{18}$$

where Q_H is the nominal horizontal tune, and a total dispersion wave of

$$\frac{\Delta\eta}{\sqrt{\beta_H}} = \frac{1}{2\ \sin(\pi Q_H)} \sum_i q_i \eta_i \sqrt{\beta_i}\ \cos(|\phi - \phi_i| - \pi Q_H) \tag{19}$$

Hence Q family jump quads at locations with small dispersions η_i generate relatively small dispersion waves.

Equations 18 and 19 show that the beta wave phase propagates twice as fast as the dispersion wave phase. Therefore, if two jump quads with the same small strength q_i are arranged in a doublet, with identical β values and spaced by 90 degrees in phase, they generate a beta wave that is localized inside the doublet. Similarly, if 4 jump quads are spaced by 90 degrees (with identical small strengths, betas, and dispersions) then both beta and dispersion waves are localized. This motivates the arrangement of Q-family jump quads in doublets, and G-family jump quads in quadruplets, as shown in Figures 1 and 2. All jump quads are located in main arc "F" CQS cryomodules, with large values of $\beta_H \approx 50$ m and small values of $\beta_V \approx 12$ m.

Unfortunately Table 1 shows that the arc FODO cells in RHIC and HSR have horizontal and vertical phase advances that are significantly smaller than 90 degrees, and so the beta and dispersion waves are not fully localized. The amount of global leakage increases with increasing deviation from 90 degrees. Further, optical distortions that are second order (and higher) in strength q_i become more important at the larger strengths that are necessary when there are fewer jump quads to generate useful $\Delta\gamma_T$ values.

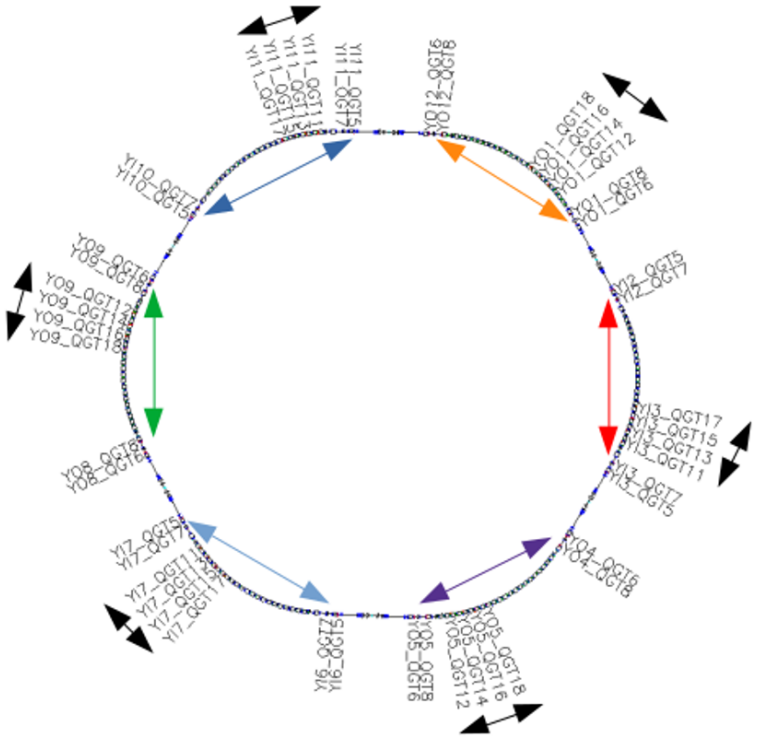

Figure 2: Twelve power supplies drive 48 jump quadrupoles in the RHIC Yellow ring. Quads at high dispersion locations are denoted by the black arrows outside the ring. Sets of low dispersion quads are marked by the colored arrows inside the ring. All jump quads appear as doublets, placed next to main arc F quads that are spaced by one FODO cell.

4 RHIC performance with 48 jump quads

Figures 1 and 2 show how each of the 6 RHIC Yellow arcs contains one G and one Q power supply. Table 2 lists the jump quad Twiss functions β_H and η generated by an optics code like BMAD or MADX. It also lists the individual power supply sensitivities S_Q and S_G that are generated via Equation 11, and which are shown graphically in Figure 3. Finally, the power supply sensitivities are summed to produce the T-matrix elements listed at the bottom-right of Table 2.

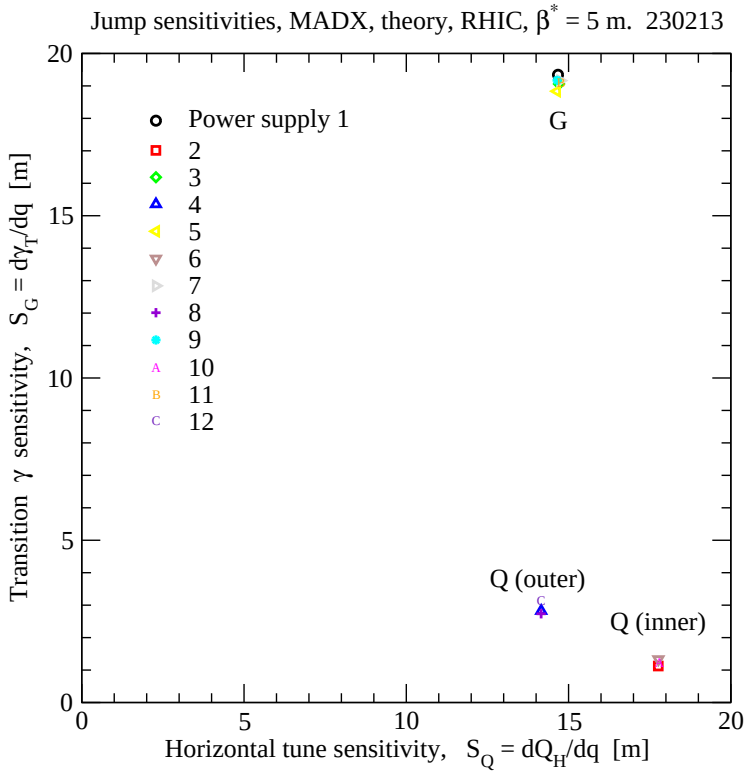

Figure 3: Sensitivities S_G and S_Q for the RHIC Yellow jump quad power supplies, with $\beta^* = 5$ m at each IP. All 6 S_G values are similar, while the S_Q values are somewhat different in the inner and outer arcs.

The 2-knob T matrix for RHIC in Table 2 is

$$T = \begin{pmatrix} T_{GG} & T_{GQ} \\ T_{QG} & T_{QQ} \end{pmatrix} = \begin{pmatrix} 114.689 & 12.385 \\ 88.171 & 95.797 \end{pmatrix} \tag{20}$$

where all elements have the dimensions of meters. The elements in its inverse

$$T^{-1} = \begin{pmatrix} 0.009681 & -0.001252 \\ -0.008911 & 0.011591 \end{pmatrix} \tag{21}$$

all have the dimensions of inverse meters. If the desired ΔQ_H is zero, then

$$\begin{pmatrix} q_G \\ q_Q \end{pmatrix} = \begin{pmatrix} 0.009681 \\ -0.008911 \end{pmatrix} \Delta\gamma_T \quad [\mathrm{m}^{-1}] \tag{22}$$

and so the maximum value of $q = 0.00833$ m^{-1} recorded in Table 1 predicts a potential $\Delta\gamma_T$ range of

$$|\Delta\gamma_T| < \frac{0.00833}{0.009681} \approx 0.86 \tag{23}$$

if the linear model holds. However, nonlinearities are significant. An optics code must be used to properly include nonlinear effects, and to test the accuracy of this linear prediction.

PS index	PS name	Quad name	Quad Twiss functions					Quad sensitivities		Power supply sensitivities G		Q	
p			β_H m	β_V m	η_H m	μ_H rad	μ_V rad	S_Q m	S_G m	S_Q m	S_G m	S_Q m	S_G m
1	yo1-qgt-ps	yo1-qgt18	47.14	10.28	1.693	103.999	110.912	3.751	4.822	14.675	19.344		
		yo1-qgt16	44.96	10.40	1.724	105.487	112.426	3.577	4.997				
		yo1-qgt14	48.03	10.26	1.700	106.904	113.944	3.822	4.861				
		yo1-qgt12	44.29	10.42	1.665	108.375	115.460	3.525	4.663				
2	yi2-qgt-ps	yi2-qgt5	64.12	5.18	-0.202	120.382	127.113	5.103	0.068			17.765	1.125
		yi2-qgt7	47.27	11.92	0.529	121.436	128.766	3.762	0.470				
		yi3-qgt7	48.15	12.13	0.578	141.483	149.934	3.831	0.561				
		yi3-qgt5	63.70	5.08	-0.124	142.529	151.590	5.069	0.026				
3	yi3-qgt-ps	yi3-qgt17	47.82	10.20	1.642	134.368	142.481	3.806	4.535	14.704	19.059		
		yi3-qgt15	44.50	10.67	1.681	135.791	143.981	3.541	4.752				
		yi3-qgt13	47.17	10.15	1.719	137.281	145.489	3.754	4.969				
		yi3-qgt11	45.29	10.73	1.690	138.690	146.994	3.604	4.803				
4	yo4-qgt-ps	yo4-qgt6	46.06	15.39	0.074	150.320	158.990	3.665	0.009			14.158	2.825
		yo4-qgt8	42.95	12.14	0.895	151.641	160.269	3.418	1.348				
		yo5-qgt8	43.28	12.01	0.934	170.466	179.607	3.444	1.466				
		yo5-qgt6	45.63	15.36	0.025	171.791	180.907	3.631	0.001				
5	yo5-qgt-ps	yo5-qgt18	46.72	10.49	1.709	163.170	172.107	3.718	4.912	14.641	18.837		
		yo5-qgt16	45.28	10.26	1.643	164.658	173.619	3.604	4.541				
		yo5-qgt14	47.21	10.54	1.638	166.088	175.130	3.757	4.512				
		yo5-qgt12	44.76	10.30	1.702	167.566	176.634	3.562	4.872				
6	yi6-qgt-ps	yi6-qgt5	64.33	5.24	-0.189	2.158	4.641	5.119	0.060			17.769	1.333
		yi6-qgt7	47.58	11.79	0.589	3.204	6.307	3.786	0.583				
		yi7-qgt7	47.64	12.13	0.622	23.226	27.488	3.791	0.651				
		yi7-qgt5	63.75	5.11	-0.151	24.279	29.150	5.073	0.038				
7	yi7-qgt-ps	yi7-qgt17	48.54	10.24	1.708	16.127	20.023	3.863	4.903	14.746	19.163		
		yi7-qgt15	44.04	10.55	1.700	17.547	21.525	3.505	4.862				
		yi7-qgt13	47.75	10.21	1.674	19.035	23.039	3.800	4.709				
		yi7-qgt11	44.97	10.60	1.670	20.437	24.545	3.579	4.689				
8	yo8-qgt-ps	yo8-qgt6	46.26	15.63	0.006	32.067	36.538	3.681	6.9e-5			14.155	2.735
		yo8-qgt8	42.71	12.00	0.898	33.391	37.813	3.399	1.355				
		yo9-qgt8	42.88	11.81	0.904	52.177	57.182	3.412	1.374				
		yo9-qgt6	46.03	15.59	0.060	53.503	58.488	3.663	0.006				
9	yo9-qgt-ps	yo9-qgt18	46.40	10.70	1.660	44.898	49.660	3.692	4.634	14.647	19.173		
		yo9-qgt16	45.60	10.01	1.649	46.392	51.181	3.628	4.575				
		yo9-qgt14	47.40	10.67	1.708	47.804	52.694	3.772	4.907				
		yo9-qgt12	44.67	10.07	1.734	49.288	54.207	3.555	5.058				
10	yi10-qgt-ps	yi10-qgt5	63.98	5.20	-0.139	61.291	65.855	5.091	0.033			17.797	1.219
		yi10-qgt7	47.96	11.94	0.581	62.335	67.538	3.817	0.568				
		yi11-qgt7	47.91	11.78	0.558	82.329	88.742	3.813	0.524				
		yi11-qgt5	63.79	5.25	-0.236	83.376	90.397	5.076	0.093				
11	yi11-qgt-ps	yi11-qgt17	48.41	10.39	1.692	75.234	81.266	3.853	4.813	14.758	19.113		
		yi11-qgt15	44.10	10.45	1.633	76.649	82.786	3.509	4.486				
		yi11-qgt13	47.67	10.36	1.672	78.141	84.281	3.793	4.701				
		yi11-qgt11	45.27	10.36	1.744	79.538	85.806	3.602	5.113				
12	yo12-qgt-ps	yo12-qgt6	46.23	15.19	0.030	91.169	97.784	3.679	0.002			14.153	3.148
		yo12-qgt8	42.91	12.13	0.971	92.485	99.087	3.415	1.584				
		yo1-qgt8	42.81	12.11	0.960	111.270	118.434	3.407	1.551				
		yo1-qgt6	45.91	15.35	0.084	112.604	119.725	3.653	0.012				
								Σ	$T_{QG} =$	88.17			
								Σ	$T_{GG} =$		114.69		
								Σ	$T_{QQ} =$			95.80	
								Σ	$T_{GQ} =$				12.39

Table 2: Jump quad and power supply sensitivities in the RHIC Yellow ring with the 2023 layout. The corresponding optical parameters, listed in Table 1, have $\beta^* = 5$ m in both planes at every IP.

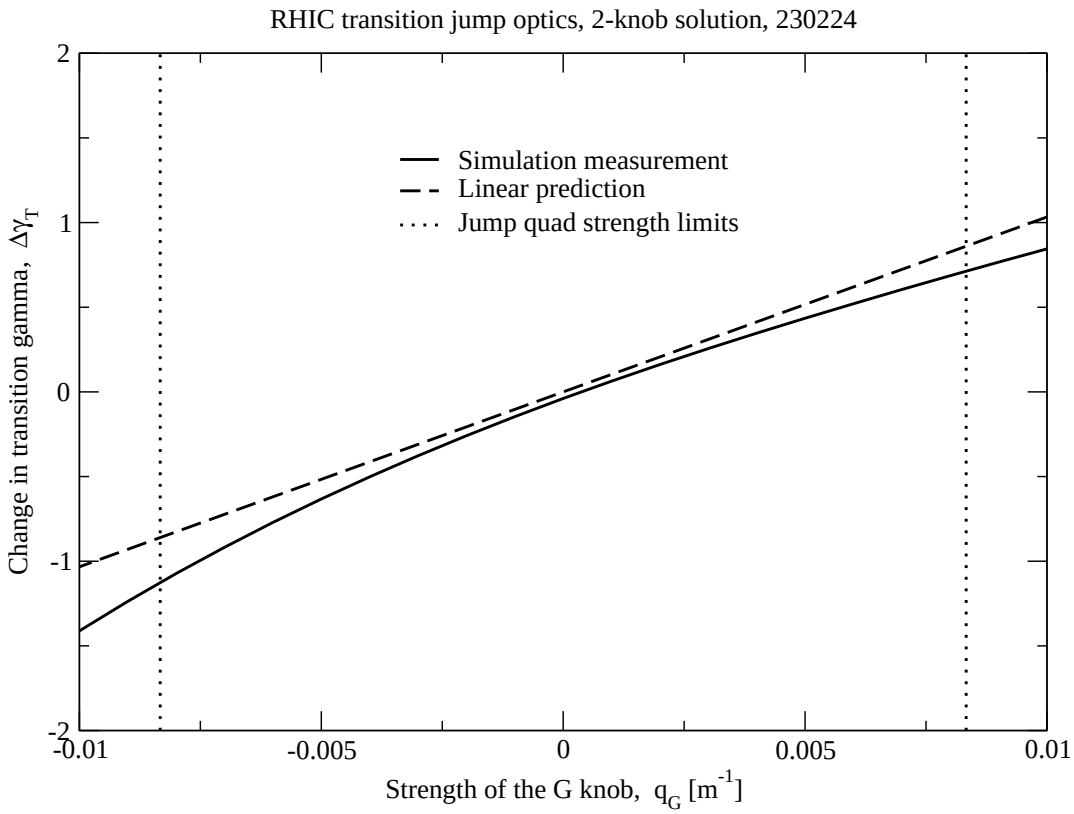

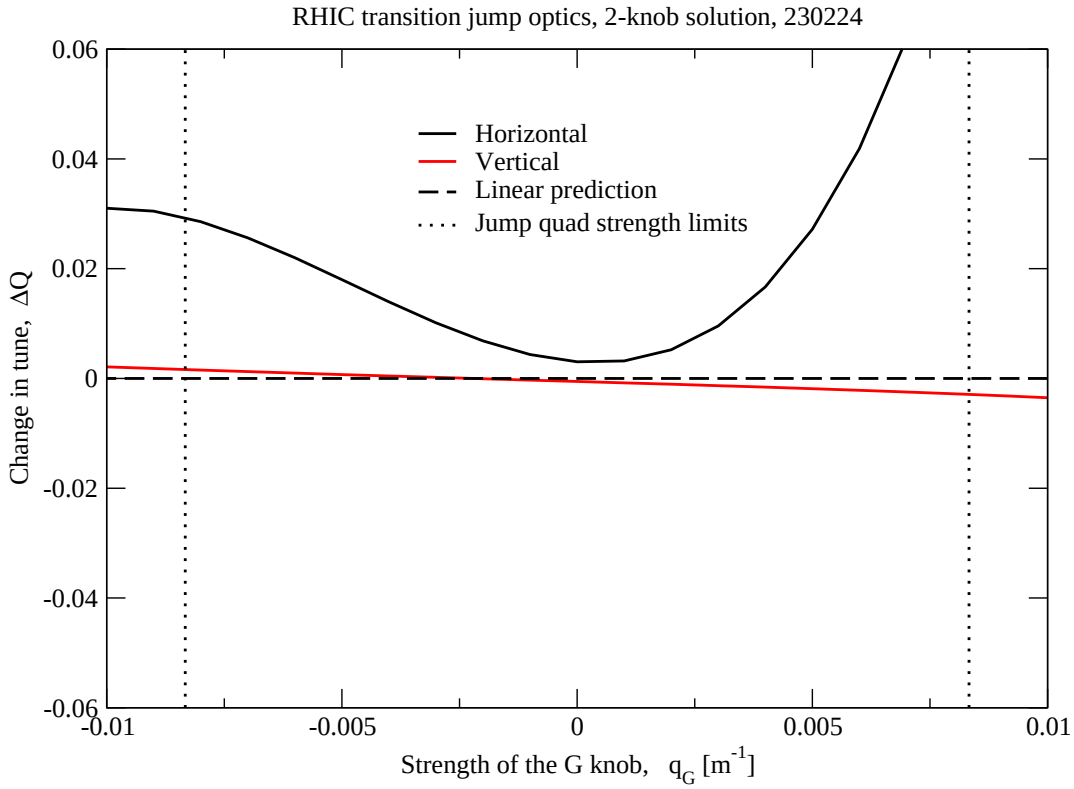

Figure 4: Optical performance in a 2-knob linear jump scheme in the RHIC Yellow ring with the 2023 layout, in transition optics with $\beta^* = 5$ m in both planes at all IPs.

Figure 4 shows results from a scan of the G family strength across the range

$$-0.01\ [\mathrm{m}^{-1}] \ < \ q_G \ < \ 0.01\ [\mathrm{m}^{-1}] \tag{24}$$

always with

$$q_Q \ = \ \frac{-0.008911}{0.009681}\, q_G \ = \ -0.921\, q_G \tag{25}$$

in order to deliver the 2-knob solution of Equation 22. The top plot shows that $\Delta\gamma_T$ is reasonably linear in q_G over power supply range of ± 50 A [5], with

$$\begin{aligned} |q_G| \ &\leq \ 0.00833 \quad [\mathrm{m}^{-1}] \\ |q_Q| \ &\leq \ 0.00767 \quad [\mathrm{m}^{-1}] \end{aligned} \tag{26}$$

These power supply limits lead to a more realistic range of

$$-1.14 \ \lesssim \ \Delta\gamma_T \ \lesssim \ 0.71 \tag{27}$$

The bottom plot shows that the desire for $\Delta Q_H = 0$ is only reasonably well met over the power supply range. Further suppression of ΔQ_H requires a 4-knob solution.

Figure 5 shows the global maximum values of β_H, β_V, and dispersion η in the distorted optics, as a function of $\Delta\gamma_T$. The distortions are significant, but tolerable. Their 2-knob values are reasonably consistent with those of the 4-knob scheme that is routinely used in RHIC operations.

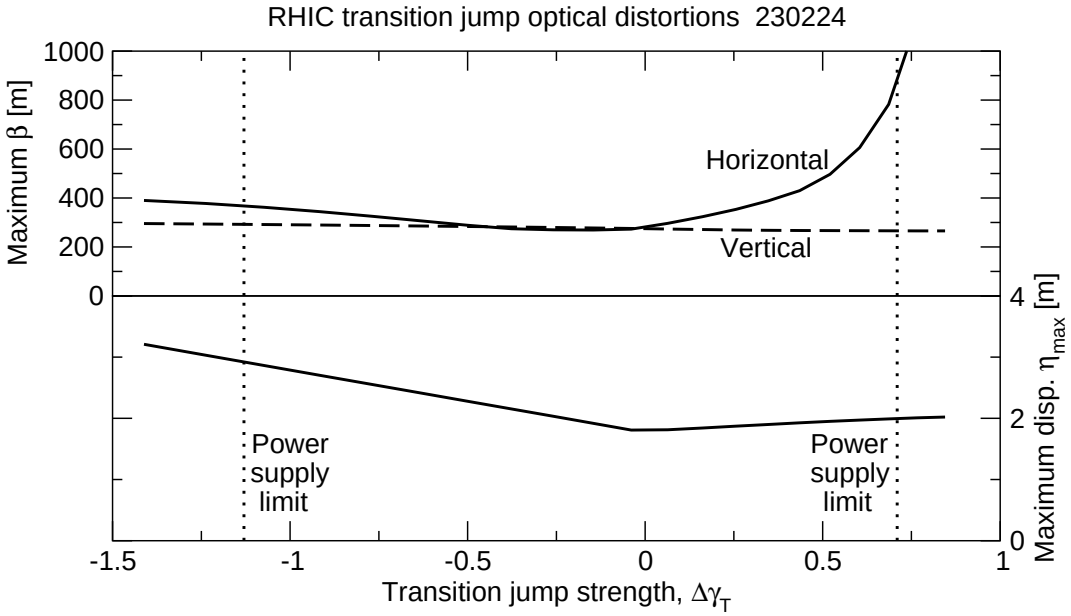

Figure 5: Optical distortions in a 2-knob linear jump scheme in the RHIC Yellow ring with the 2023 layout, and optics with $\beta^* = 5$ m in both planes at all IPs.

5 HSR performance with 38 jump quads

Figure 6 shows where the HSR lost 10 jump quads, compared to the RHIC layout in Figure 2. Six G power supplies still drive 4 quads, but now there are only 5 Q power supplies, 3 of which drive only 2 quads.

Table 3 records the HSR power supply sensitivities and shows that the net 2-knob T matrix is

$$T = \begin{pmatrix} T_{GG} & T_{GQ} \\ T_{QG} & T_{QQ} \end{pmatrix} = \begin{pmatrix} 111.892 & 9.338 \\ 87.582 & 55.280 \end{pmatrix} \tag{28}$$

where all matrix elements have the dimensions of meters. All elements in the inverse matrix

$$T^{-1} = \begin{pmatrix} 0.010299 & -0.001740 \\ -0.016317 & 0.020846 \end{pmatrix} \tag{29}$$

have the dimensions of inverse meters. If the desired ΔQ_H is zero, then

$$\begin{pmatrix} q_G \\ q_Q \end{pmatrix} = \begin{pmatrix} 0.010299 \\ -0.016317 \end{pmatrix} \Delta\gamma_T \ \ [\mathrm{m}^{-1}] \tag{30}$$

and so the maximum value of q recorded in Table 1 predicts a potential $\Delta\gamma_T$ range of

$$|\Delta\gamma_T| < \frac{0.00877}{0.016317} \approx 0.54 \tag{31}$$

insofar as the linear model holds.

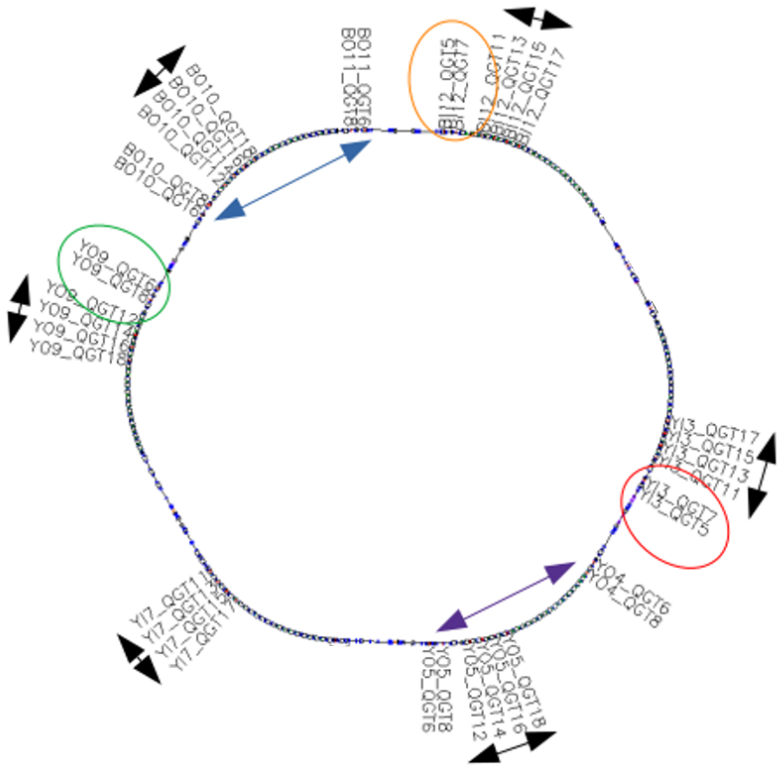

Figure 6: The layout of the 11 transition jump power supplies and 38 jump quads in the preliminary HSR layout EIC-HSR-20220921a that was prepared for 275 GeV proton squeezed collisions at IP6 and IP8. Some or all of the 10 quads that have been eliminated need to be restored. Six G power supplies drive quadruplets of high dispersion quads at the locations indicated by the black arrows outside the ring. Two Q power supplies that drive 4 low dispersion jump quads are indicated by colored arrows inside the ring. The 3 Q power supplies that drive only 2 jump quads are indicated by colored ellipses.

PS index	PS name	Quad name	Quad Twiss functions					Quad sensitivities		Power supply sensitivities G		Q	
p			β_H m	β_V m	η_H m	ϕ_H rad	ϕ_V rad	S_Q m	S_G m	S_Q m	S_G m	S_Q m	S_G m
1	bi1-qgt-ps	bi12-qgt5	63.34	6.87	-0.317	98.381	91.559	5.040	0.141			8.816	0.629
		bi12-qgt7	47.45	11.16	0.589	99.403	93.078	3.776	0.487				
2	yi2-qgt-ps	yi3-qgt5	66.07	6.55	-0.321	144.208	137.034	5.258	0.145			8.891	0.592
		yi3-qgt7	45.66	11.67	0.564	143.188	135.484	3.634	0.446				
3	yi3-qgt-ps	yi3-qgt11	44.77	11.83	1.802	140.453	132.663	3.562	4.565	14.250	18.260		
		yi3-qgt13	44.77	11.83	1.802	139.080	131.244	3.562	4.565				
		yi3-qgt15	44.77	11.83	1.802	137.706	129.826	3.562	4.565				
		yi3-qgt17	44.77	11.83	1.802	136.333	128.408	3.562	4.565				
4	yo4-qgt-ps	yo4-qgt6	39.87	16.70	-0.074	152.464	144.070	3.172	0.008			15.936	3.225
		yo4-qgt8	44.88	11.87	1.089	153.911	145.373	3.572	1.666				
		yo5-qgt6	74.47	33.97	0.414	172.666	164.398	5.926	0.240				
		yo5-qgt8	41.05	19.04	0.966	171.822	163.502	3.267	1.311				
5	yo5-qgt-ps	yo5-qgt12	46.95	11.20	1.840	169.014	160.819	3.736	4.759	14.945	19.037		
		yo5-qgt14	46.95	11.20	1.840	167.636	159.396	3.736	4.759				
		yo5-qgt16	46.95	11.20	1.840	166.259	157.973	3.736	4.759				
		yo5-qgt18	46.95	11.20	1.840	164.881	156.551	3.736	4.759				
6	NONE							0.000	0.000				
7	yi7-qgt-ps	yi7-qgt11	44.77	11.83	1.802	22.326	21.710	3.562	4.565	14.250	18.260		
		yi7-qgt13	44.77	11.83	1.802	20.952	20.291	3.562	4.565				
		yi7-qgt15	44.77	11.83	1.802	19.579	18.873	3.562	4.565				
		yi7-qgt17	44.77	11.83	1.802	18.205	17.454	3.562	4.565				
8	yo8-qgt-ps	yo9-qgt6	48.63	14.05	0.109	58.006	58.012	3.870	0.017			7.446	1.603
		yo9-qgt8	44.94	13.51	1.063	56.777	56.789	3.576	1.587				
9	yo9-qgt-ps	yo9-qgt12	46.95	11.20	1.840	54.007	54.008	3.736	4.759	14.945	19.037		
		yo9-qgt14	46.95	11.20	1.840	52.630	52.585	3.736	4.759				
		yo9-qgt16	46.95	11.20	1.840	51.252	51.163	3.736	4.759				
		yo9-qgt18	46.95	11.20	1.840	49.875	49.740	3.736	4.759				
10	bo10-qgt-ps	bo10-qgt12	44.88	11.80	1.799	73.578	67.744	3.571	4.547	14.286	18.188		
		bo10-qgt14	44.88	11.80	1.799	74.955	69.166	3.571	4.547				
		bo10-qgt16	44.88	11.80	1.799	76.332	70.589	3.571	4.547				
		bo10-qgt18	44.88	11.80	1.799	77.710	72.011	3.571	4.547				
11	bo11-qgt-ps	bo10-qgt6	46.67	14.73	0.115	69.578	63.731	3.714	0.019			14.190	3.289
		bo10-qgt8	42.97	14.13	1.043	70.808	64.955	3.420	1.530				
		bo11-qgt6	41.73	16.05	-0.086	90.128	84.479	3.321	0.010				
		bo11-qgt8	46.95	11.27	1.110	88.681	83.189	3.736	1.731				
12	bi12-qgt-ps	bi12-qgt11	46.83	11.23	1.844	102.138	95.899	3.727	4.778	14.907	19.111		
		bi12-qgt-13	46.83	11.23	1.844	103.512	97.318	3.727	4.778				
		bi12-qgt-15	46.83	11.23	1.844	104.885	98.736	3.727	4.778				
		bi12-qgt-17	46.83	11.23	1.844	106.258	100.155	3.727	4.778				
								Σ	T_{QG} =	87.582			
								Σ	T_{GG} =		111.892		
								Σ	T_{QQ} =			55.280	
								Σ	T_{GQ} =				9.338

Table 3: Jump quad and power supply sensitivities in the HSR layout EIC-HSR-20220921a, with nominal optics for two squeezed collisions of 275 GeV protons. Six G power supplies each drive 4 quads, as in RHIC. There are only 5 Q power supplies, 3 of which drive only 2 quads, for a net reduction of 10 jump quads.

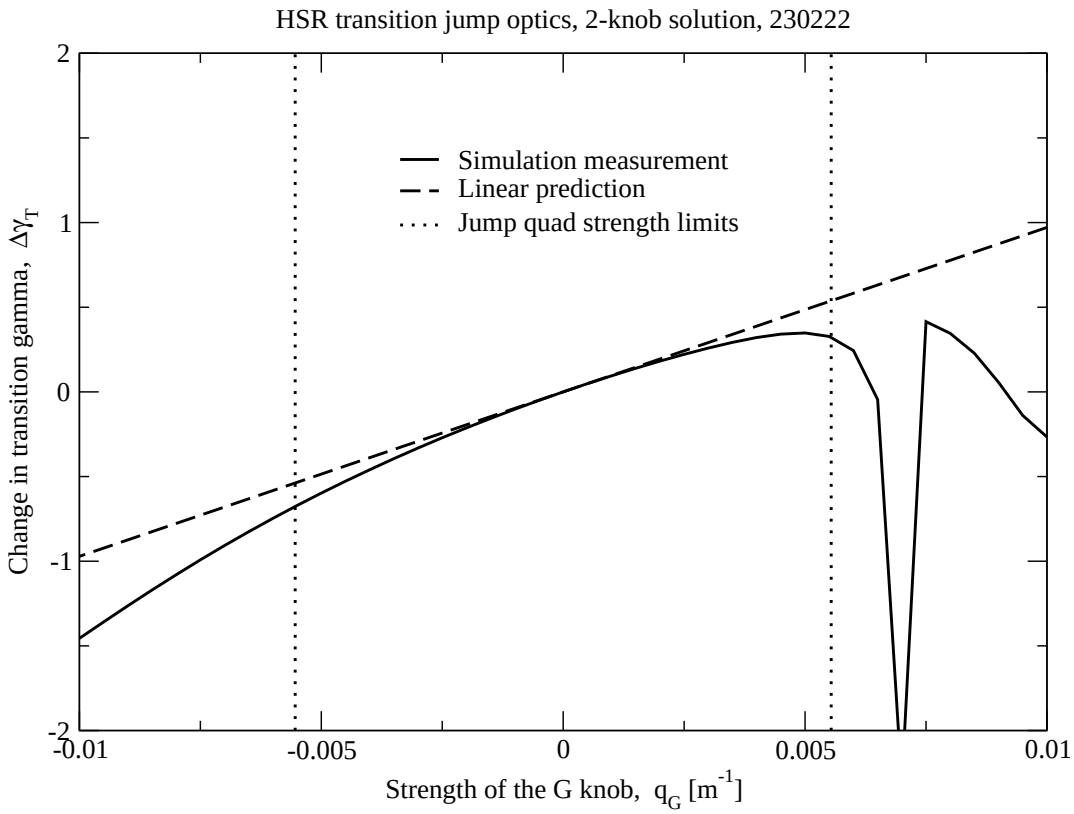

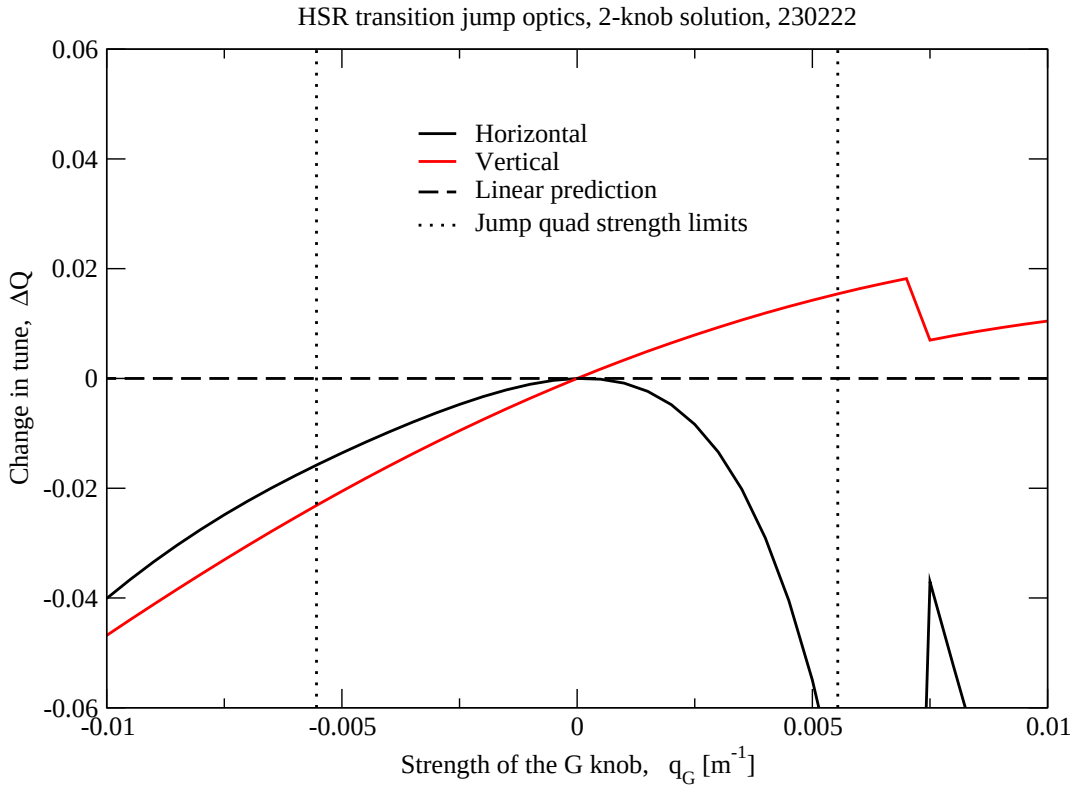

Figure 7: Optical distortions in a 2-knob linear jump scheme in the HSR with layout EIC-HSR-20220921a and squeezed 2-collision optics.

Figure 7 tests this prediction. It shows results from a scan of the G family strength across the range

$$-0.01\,[\mathrm{m}^{-1}] \;<\; q_G \;<\; 0.01\,[\mathrm{m}^{-1}] \tag{32}$$

always with

$$q_Q \;=\; \frac{-0.016317}{0.010299}\,q_G \;=\; -1.584\,q_G \tag{33}$$

in order to deliver the 2-knob solution of Equation 30. The top plot in Figure 7 shows that $\Delta\gamma_T$ is reasonably linear in q_G, but with a saturated response at about $q_G \approx 0.005$, and with unstable optics at about $q_G \approx 0.007$, just beyond the power supply limits of

$$\begin{aligned} |q_G| &\leq 0.00554 \quad [\mathrm{m}^{-1}] \\ |q_Q| &\leq 0.00877 \quad [\mathrm{m}^{-1}] \end{aligned} \tag{34}$$

Nonlinear deviations from the linear model lead to a more realistic range of

$$-0.69 \;\lesssim\; \Delta\gamma_T \;\lesssim\; 0.34 \tag{35}$$

at the extremes of jump quad capabilities. The bottom plot in Figure 7 shows that the desire for $\Delta Q_H = 0$ is not as well met as in RHIC, and that the ΔQ_V behavior is much worse. It is not clear that a 4-knob solution could remediate these problems in the HSR.

Figure 8 shows the optical distortions of β_H, β_V, and dispersion η, as a function of $\Delta\gamma_T$. The β-functions here are much larger in general than in Figure 5, because the HSR results use collision optics, while the RHIC results use optimized transition crossing optics.

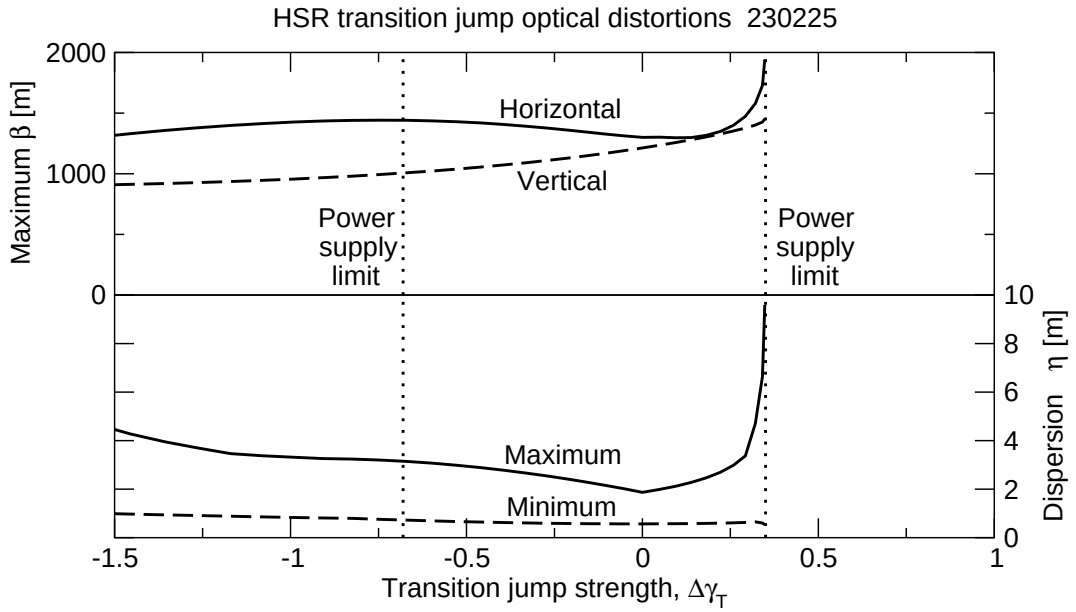

Figure 8: Optical distortions in a 2-knob linear jump scheme in the HSR with layout EIC-HSR-20220921a and squeezed 2-collision optics.

6 Comparing HSR-38 and RHIC-48

Table 4 summarizes how HSR performs with 38 jump quads, compared to RHIC performance with 48 jump quads, in the 2-knob scenario.

Missing Q jump quads. All 10 of the jump quads that were displaced in developing HSR-38 from RHIC-48 were lost from low-dispersion locations, where Q jump quads reside. Consequently the 2-knob sensitivity T_{QQ} is approximately halved, going from 95.8 m in RHIC to 55.3 m in HSR. This makes it necessary for the Q-family strength $|q_Q|$ to be 1.584 times larger than the G-family strength $|q_G|$ in the HSR. The opposite is true in RHIC, where $|q_Q| = 0.921|q_G|$.

Parameter		**Units**	**RHIC-48**	**HSR-38**
Number of jump quads G			24	24
Q			24	14
2-knob sensitivity T_{GG}		m	114.7	111.9
T_{QQ}		m	95.8	55.3
2-knob strength ratio, q_Q/q_G			-0.921	-1.584
Maximum jump quad strength $\|q_G\|$		m^{-1}	0.00833	0.00554
$\|q_Q\|$		m^{-1}	0.00737	0.00877
$\Delta\gamma_T$ range, linear prediction,	max/min		±0.86	±0.54
simulated,	min		-1.13	-0.68
	max		0.71	0.35
	span		1.84	1.03
ΔQ range, linear prediction,	H span		0	0
simulated,	H min		0	-0.075
	H max		0.102	0
	H span		0.102	0.075
linear prediction,	V span		–	–
simulated,	V min		-0.003	-0.023
	V max		0.002	0.015
	V span		0.005	0.038
Optical distortions, β_{max},	H min	m	269	1297
	H nominal	m	273	1300
	H max	m	884	1939
	V min	m	266	1005
	V nominal	m	275	1213
	V max	m	292	1451
η_{max},	min	m	1.81	1.87
	nominal	m	1.81	1.87
	max	m	2.91	9.57

Table 4: Transition crossing optical performance in RHIC-48 and HSR-38. Linear predictions are calculated in the 2-knob scenario. Minimum and maximum simulated values of $\Delta\gamma_T$ and ΔQ are calculated across the achievable range of jump quad strengths q. These extreme strengths occur when a current of ±50 A delivers an integrated strength of $|B'L| = 1.5$ T at the appropriate transition rigidity [5]. The maximum of $|q_G|$ and $|q_Q|$ differs slightly between RHIC-48 and HSR-38 (with values 0.00833 and 0.00877 m^{-1}) because γ_{T0} differs slightly between RHIC and HSR, as noted in Table 1.

Range of $\Delta\gamma_T$. In consequence the linearly predicted range of $\Delta\gamma_T$ drops from ± 0.86 in RHIC to ± 0.54 in HSR, with predicted total spans of twice that: 1.72 and 1.08 in RHIC and HSR, respectively. Nonlinearities (with respect to q) are important in both RHIC and HSR. Simulations show that they change the predicted span to 1.84 in RHIC, and 1.03 in HSR. The loss in $\Delta\gamma_T$ span from RHIC to HSR is significant.

Asymmetric jumps. The loss in $\Delta\gamma_T$ span is somewhat ameliorated by the fact that the response curves – in $\Delta\gamma_T, \Delta Q_H, \Delta Q_V, \beta_{H,max}, \beta_{V,max}$, and η_{max} versus $\Delta\gamma_T$ – are asymmetric about $\Delta\gamma_T = 0$. In consequence the fast jump in HSR could be centered around a non-zero (negative) value of $\Delta\gamma_T$, as it is already in RHIC operations.

Tune shifts. The horizontal and vertical tune shifts span a range of 0.102 and 0.005 in RHIC, and 0.075 and 0.038 in HSR, over the full power supply range. This is a significant concern in RHIC operations, where it is satisfactorily ameliorated by using a 4-knob scheme, while no further attention to vertical tune shifts, which are already negligibly small in the 2-knob scheme. By contrast, both vertical and horizontal tune shifts in HSR need further attention in the HSR, for example by implementing a 4-knob solution, eventually.

Optical distortions. Optical distortions are a major concern. Table 4 shows that $\beta_{V,max}$ and η_{max} values in RHIC are relatively well-controlled, varying only from 266 m to 292 m, and from 1.81 m to 2.91 m, over the full power supply range. Distortions of $\beta_{H,max}$ in RHIC are large, varying from 269 m to 884 m. Optical distortions in HSR are in general larger, with $\beta_{V,max}$ and η_{max} varying from 1005 m to 1451 m, and from 1.87 m to 9.57 m, respectively. Nonetheless $\beta_{H,max}$ distortions in HSR are better than in RHIC, with values varying from 1297 m to 1939 m.

7 Summary of potential avenues for future work

This technical note analyses the loss in transition crossing performance that occurred during the early development of the HSR layout, and collision optics. Insofar as there is little "head room" in the current RHIC first order jump scheme, the question becomes: **How to restore RHIC performance in the HSR?** There are several potential directions for future work aimed at achieving this restoration. The following unordered and partial list describes potential avenues:

1. **Updating the jump quad distribution.** This necessitates moving CQS modules around, for example by reinstalling elsewhere modules with jump quads that are decommissioned from the Blue ring. Some or all of the 10 missing Q jump quads (see Table 4) could be replaced. The jump quads in the two Blue arcs (see Figure 6) could be relocated at the other end of their respective arcs, in order to maintain the RHIC layout of the G families and reestablish phase advance intervals between thems

2. **Increasing the integer tunes for ions, but not for protons.** Optical distortions become more severe, the further the horizontal and vertical phase advances per main arc FODO cell deviate from 90 degrees. These phase advances were further reduced from 90 degrees in the HSR optics analyzed here, in part to enable the highest possible proton collision energies (see Table 1). However, protons do not cross transition, and achieving the highest possible energy is not a concern for ions like gold. Thus, ion optics could include larger integer tunes than proton optics, with larger phases advance per FODO cell and milder optical distortions around jump time. This could restore RHIC transition crossing performance, provided that the necessary increase in Q and G strengths (with 10 missing Q jump quads) is achievable.

3. **Developing transition (and injection) optics.** At the time of writing only one optic has been officially released for the EIC-HSR-20220921a layout, for proton-electron collisions with two collision points. This explains the anomalously large β_{max} values shown in Figure 7, and listed in Table 4. In practice the HSR will cross transition in optics that are closely similar to injection optics, just as in RHIC. Transition optics may well ameliorate the optical distortions reported here for HSR-38.

4. **Blue quadrupole quench diode polarity.** If the main arc quadrupole quench diodes are *not* reversed in the Blue ring, then Blue jump quads will no longer be at F locations with large values of $\beta_H \approx 50$ m and $\eta \approx 2$ m, but at D locations with small values of $\beta_H \approx 12$ m and $\eta \approx 1$ m. Equation 11 shows that this would weaken both S_G and S_Q sensitivities by a factor of about 4, for the 14 jump quads that Table 3 lists in the Blue ring. This would further impair the performance of the HSR jump scheme.

5. **Alternate schemes.** The first order transition jump scheme in RHIC could be abandoned for use in HSR, in favor of an alternate scheme. For example, a second order jump scheme could be invoked. Recently "A novel non-adiabatic approach to transition crossing in a circular hadron accelerator" was proposed by Giovannozzi et al, for potential use in the CERN SPS [7]. It follows some of the concepts implemented in Multi-Turn Extraction, as routinely performed in the CERN PS. Such a resonance island scheme could also be evaluated for use in HSR.

6. **Beam simulations.** This note explicitly "doesn't care about beam or time", in favor of focusing on static optical performance. Sooner or later fuller simulations need to be performed, including longitudinal motion, accelerating beam with realistic parameters through transition in the presence of errors.

7. **Beam studies.** RHIC transition crossing studies could be performed with 8 or 12 Q jump quads turned off, to better emulate HSR-38. The fundamentals of the alternative scheme proposed by Giovannozzi et al [7] could first be tested by injecting into open islands, with no additional instrumentation. If early studies are successful, and if appropriate instrumentation is in place, then later studies could include crossing transition with beam stored in resonance islands.

Not all of these avenues need to be explored. Their relative prioritization is not clear at the time of writing.

Acknowledgements

Many thanks to Massimo Giovannozzi for stimulating discussions about a potential alternative scheme for crossing transition in the HSR and in the CERN SPS, and to Chuyu Liu for discussions about RHIC capabilities in potentially performing beam tests to validate some of these ideas.

References

[1] Johnsen K. 1956. Effects of nonlinearities on the phase transition. *CERN Symposium on HE Accels. and Pion Physics* 1:106

[2] Takayama K. 1984. *Part. Accel.* 14:201

[3] Kewisch J, Tang C. 2001. RHIC optics for transition jump *C-A/AP/53* BNL.

[4] Bogacz SA, Peggs S. 1991. Comments on the behavior of α_1 in Main Injector transition Jump Schemes *Part. Accel. Conf.* p. 1657

[5] 2006. RHIC Configuration Manual. Table 11-4, p. 25

[6] Harrison M, Peggs S, & Roser T. 2002. The RHIC accelerator. *Annu. Rev. Nucl. Part. Sci.* Vol. 52, p. 425

[7] Giovannozzi et al. 2021. A novel non-adiabatic approach to transition crossing in a circular hadron accelerator. *Eur. Phys. J. Plus (2021) 136:1189*